Applied Catalysis B: Environmental 216 (2017) 1–10

Contents lists available at ScienceDirect

Applied Catalysis B: Environmental

journal homepage: www.elsevier.com/locate/apcatb

Electronic state of silver in Ag/SiO^2 and Ag/ZnO catalysts and its effect on diesel particulate matter oxidation: An XPS study

Grisel Corro[a,*], Esmeralda Vidal[b], Surinam Cebada[a], Umapada Pal[c], Fortino Bañuelos[a], Diana Vargas[d], Emmanuel Guilleminot[e]

[a] Instituto de Ciencias, Benemérita Universidad Autónoma de Puebla, 4 sur 104, 72000, Puebla, Mexico, Mexico
[b] Facultad de Ingeniería Química, Benemérita Universidad Autónoma de Puebla, 4 sur 104, 72000, Puebla, México
[c] Instituto de Física, Benemérita Universidad Autónoma de Puebla, Apdo. Postal J-48, 72570 Puebla México
[d] Universidad de Sonora, Calle Rosales S/N 83000 Hermosillo, Sonora, México
[e] Universidad de las Américas Puebla, Sta. Catarina Mártir, San Andrés, Cholula, Puebla, México

ARTICLE INFO

Article history:
Received 25 April 2017
Accepted 20 May 2017
Available online 22 May 2017

Keywords:
Ag/SiO_2
Ag/ZnO
Diesel particulate matter oxidation
Ag^0 catalytic site
Ag^{1+} catalytic site
Diesel combustion

ABSTRACT

Diesel particulate matter (DPM) oxidation activities of 3%Ag/SiO_2 and 3%Ag/ZnO catalysts were investigated. The catalysts were characterized by X-ray diffraction, X-ray photoelectron spectroscopy (XPS) and diffuse reflectance spectroscopy (DRS). 3%Ag/SiO_2 showed excellent activity for DPM oxidation below 300 °C. The high activity is attributed to the presence of Ag^0 at the surface of SiO_2, which enhances the generation of superoxide O_2^-, the highly active species in the oxidation reactions. The activity of the catalyst did not change up to 6 oxidation cycles, indicating there is no change in electronic state of Ag during high temperature oxidation of DPM. However, 3%Ag/ZnO exhibited a very low DPM oxidation activity at the studied temperature range (25–600 °C). XPS analysis performed on the catalysts before and after their use in DPM oxidation revealed that a fraction of Ag^0 in the 3%Ag/ZnO converts to Ag^{1+} state, probably due to the electron transfer from the Fermi level of the low work function metallic Ag to the conduction band of high band gap n-type semiconductor ZnO. We demonstrate a direct relation between the DPM oxidation activity of silver and its electronic state at the catalyst surface.

1. Introduction

Diesel technology achieved a great advancement over the past decades owing to the efficient energy conversion of diesel engine [1]. However, emission of particulate matter from diesel vehicles (DPM), which consists mostly of carbonaceous soot as major environmental pollutant, causes acute health problems to humans and animals. Consequently, a diesel particulate filter which can collect more than 90% of DPM has been employed [2]. The most challenging task in this regard is the simultaneous in-situ regeneration of the filter by combustion of trapped DPM. Accordingly, active regeneration of filter requires a higher temperature (ca. 550–600 °C) than that of exhaust gas temperature (200–400 °C) of a diesel engine [3].

Use of a catalyst is the key to lower the ignition temperature of the trapped DPM [4]. Among the available technologies for filter regeneration, addition of the catalysts to the fuel in the form of organic derivates of active metals, known as fuel-borne catalysts (FBCs) and the deposition of a catalytic coating onto the filter surface are the most popular ones. While in both of these technologies, soot particle combustion occurs at lower temperatures [5], the continuous consumption of FBCs and the accumulation of metal oxide ash inside the filter restrict their applications [6].

Catalyzed diesel particulate filter is regarded as the most viable solution to reduce DPM emissions. In the filter, DPM is trapped and oxidized with a catalyst at lower temperature. The major problem with this filter is the poor contact between the catalyst surface and the particulates [7]. To overcome this problem, the so-called continuously regeneration trap (CRT) has been developed [8]. In this technology, a NO_2 gaseous flux, generated from the oxidation of NO over a platinum catalyst, functions as a mobile species for DPM oxidation by creating catalyst-DPM contact. However, the new trend of diesel engines to decrease NO_x emission could prevent the application of this technology.

Transition metals [9], transition metal oxides [10], alkaline metal oxides [11],perovskites [12], and rare earth oxides [13] are some of the catalysts which have exhibited good catalytic performances. The role of transition metal catalysts in DPM oxidation is to

* Corresponding author.
E-mail addresses: griselda.corro@correo.buap.mx, griselcorro@yahoo.com (G. Corro), upal@ifuap.buap.mx (U. Pal).

http://dx.doi.org/10.1016/j.apcatb.2017.05.059
0926-3373/

transfer active oxygen species from their surface to the particulates [14]. Therefore, the performance of these catalysts for DPM oxidation depends on their capacity to activate oxygen and on the contact condition between the catalysts and the particulates [15–18].

Supported silver nanoparticles as active components are an interesting choice to enhance the intrinsic catalytic performance of oxidation catalysts [16–19]. Aneggi et al. studied the effect of Ag addition on the soot oxidation activity of various metal oxides [19]. They found that the combustion of DPM is promoted by the presence of silver, especially in the zero valent state, which is favored by alumina and zirconia supports. However silver deposited on CeO_2, which favors Ag to stay in its positive electronic state, losses its activity at high temperature.

Recently we have demonstrated a high DPM oxidation capacity of hydrogen reduced Ag/SiO_2 due to the presence of metallic Ag^0 species on SiO_2 surface, which probably enhances the generation of very active superoxide O_2^- species during oxidation reactions. The low probability of electron transfer between SiO_2 and Ag due to the insulating character of SiO_2 results in the formation of very stable Ag^0 species over SiO_2 surface [20]. As the electron transfer process between the supported metal and supporting metal oxide is known to play important role in the production of metal ions of different valence states and hence the catalytic activity of supported catalysts, in this investigation, we have analyzed the valence state of silver, supported on insulating SiO_2 and on n-type semiconductor ZnO, to correlate their catalytic activity for DPM oxidation.

The structural and electronic properties of the catalysts were studied utilizing X-ray photoelectron spectroscopy (XPS), UV–vis diffuse reflectance spectroscopy (DRS), and X-ray diffraction spectroscopy (XRD) techniques. The catalytic behavior of the composites in DPM oxidation in the 25–600 °C temperature range has been correlated to their physicochemical properties, considering the interactions of active and non-active species such as Ag^0, and Ag^{1+} with oxygen and DPM, along with the interactions between Ag and the SiO_2 and ZnO supports.

2. Experimental

2.1. Catalysts preparation

SiO_2 and ZnO powders (99.99%), supplied by Aldrich, Mexico, were used as support materials. The catalysts were prepared by impregnation, using the appropriate amount of an aqueous solution of 1% silver nitrate (Aldrich, 99.99%). After impregnation, the catalysts were dried at 120 °C overnight and reduced in pure hydrogen flow (80 ml min^{-1}) for 4 h at 450 °C. After cooling down to room temperature, the samples were purged with N_2 for 30 min and stored in dry conditions, after which were named as $3\%Ag/SiO_2$ and 3%Ag/ZnO. SiO_2 and ZnO supports without $AgNO_3$ were also prepared following the same procedure, to use them as References

2.2. Catalysts characterization

A Quantachrome Nova-1000 sorptometer was used to measure the N_2 adsorption-desorption isotherms of the catalysts. Specific surface area (S_g) of the samples was estimated from their N_2 physisorptions at 77 K, using BET analysis. The samples (1 g each) were degassed at 400 °C for 2 h before recording their adsorption-desorption isotherms. After cooling to room temperature (25 °C), the isotherms were recorded in the pressure range 0.0–6.6 kPa. The technique of back extrapolation of the linear portion of the isotherms to zero equilibrium pressure was used to determine the saturation uptake.

The diffuse reflectance spectra (DRS) of the catalysts before and after 6 particulate matter oxidation cycles were measured on dry-pressed disks (~15 mm diameter) using a Shimadzu UV–vis spectrophotometer equipped with an integrating sphere, and $BaSO_4$ as standard reflectance sample. The crystallinity and structural phase of the samples were verified through powder X-ray diffraction (XRD), using the CuKα radiation (λ = 1.5406 Å) of a Bruker D8 Discover diffractometer.

X-ray photoelectron spectra were recorded on freshly prepared hydrogen reduced $3\%Ag/SiO_2$ and 3%Ag/ZnO catalysts and after their 6th particulate matter oxidation cycle, using an Escalab 200R electron spectrometer equipped with a hemispherical analyzer, operating in a constant pass energy mode. Monochromatic MgK_α emission ($h\nu$ = 1253.6 eV) from the X-ray tube operating at 10 mA and 12 kV was utilized for recording the XPS spectra of the samples. Different energy regions of interest of the photoelectrons were scanned a number of times in order to get good signal-to-noise ratios. The intensities of the emission peaks were estimated by determining the integral of each peak after subtracting an S-shaped background and fitting the experimental peak to Lorentzian/Gaussian curves (80%L/20%G). The peak positions of the elements were corrected utilizing the position of C*1 s* peak coming from adventitious carbon appeared at 284.9 ± 0.2 eV.

TEM images of the fresh $3\%Ag/SiO_2$ and 3%Ag/ZnO catalysts and after 6 oxidation cycles were obtained in a JEM 2100F microscope fitted with an INCA X-sight (Oxford Instruments) energy dispersive X-ray spectroscope (EDS), operating at 200 kV accelerating voltage.

2.3. Generation of diesel particulate matter

The particulate matter used in this study was generated by burning pure Mexican diesel acquired from local market in a glass vessel under controlled air flow, as described in Fig. 1. In this study, the term 'particulate matter' is used to refer both the soluble and insoluble (carbon) fractions of the diesel-emission.

The emission from the exhaust of the vessel was directed to the catalyst sample (200 mg) placed inside a tubular quartz reactor (inner diameter 10 mm) in a programmable furnace. The process was performed using an air feed volume flow rate of 100 cm^3 min^{-1}. The particulate matter generated from the exhaust of the vessel was accumulated on the catalyst in the tubular reactor. The resulting contact between particulate matter and the catalyst in this case was considered similar to the contact between the particulate matter generated from a real diesel engine and the catalyst used in a particulate filter. Therefore, the concept of tight mode or light mode contact between the particulate matter and the catalyst used in several research studies is of no significance here.

After 1 h of diesel combustion, the total amount of particulate matter retained by the catalysts was measured using a Shimadzu AX200 balance. To investigate the reproducibility of the quantity and composition of the DPM produced on diesel burning in the vessel, the amount of DPM retained by the different catalysts was measured after 3 accumulation processes.

To investigate the reproducibility of the composition of DPM produced in the diesel-burning vessel, the organic functional groups in the particulate matter emanating from the combustion vessel exhaust were analyzed in a Bruker FT-IR spectrometer (Vertex 70) in the 800–4000 cm^{-1} spectral range. A thin, uniform KBr pellet prepared with 0.2 wt% of the particulate matter sample was used for recording the FT-IR spectra.

The composition of the exhaust gas was determined in a Bruker (Vertex 70) FTIR gas spectrometer. The analysis of the exhaust was performed in a quartz cell (provided by Pike Technologies), and the gas composition was analyzed, using the QAsoft-quantitative Analysis Software (provided by Infrared Analysis Inc) which allowed determining the quality and quantity of the emitted gases from the vessel exhaust.

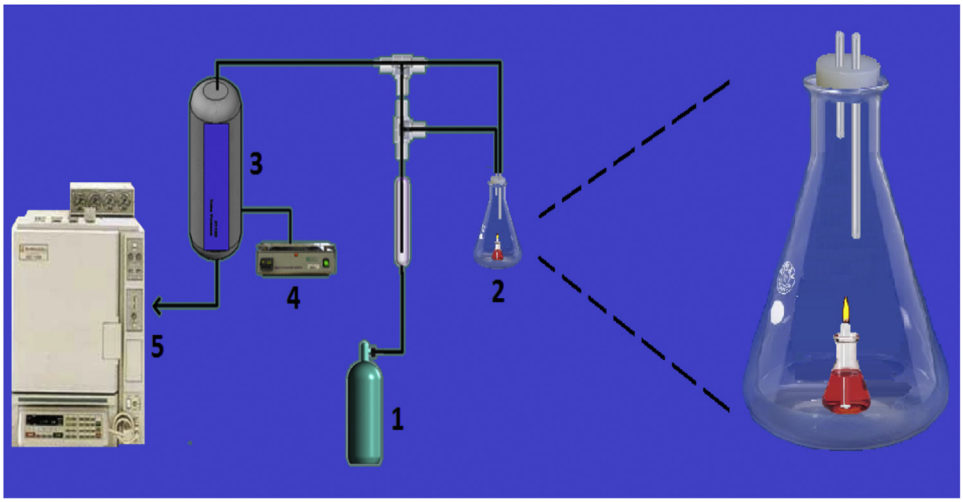

Fig. 1. Schematic diagram of the system used for monitoring the combustion process. 1: Air; 2: Diesel burner; 3: Reactor; 4: Temperature controller; 5: Gas chromatograph.

2.4. Particulate matter oxidation through programmed temperature experiments

After the accumulation of diesel particulate matter over catalyst surface, air was purged for 15 min to remove weakly attached combustion products. The air (20 vol% of O_2 and 80 vol% of N_2) flow rate was maintained at 100 $cm^3 \cdot min^{-1}$. The mixture was then heated from room temperature (25 °C) to 600 °C at the rate of 5 °C•min^{-1}. A thermocouple was inserted into the particulate matter-catalyst mixture to monitor its temperature along with the exothermic heat of the particulate matter oxidation. The emissions from the reactor were analyzed every 5 min through a computer programmed Shimadzu gas chromatograph provided with a thermo-conductivity detector (TCD) to monitor the CO_2 evolution at different temperatures. The chromatograph was fitted with a Porapak column to analyze CO_2 evolutions as a function of the temperature of the particulate matter-catalyst mixture. The process comprising particulate matter accumulation on the catalyst at room temperature (during 1 h), its subsequent oxidation at high temperature, and then cooling down to 25 °C is designated as a cycle. The duration of each cycle was about 2.5 h. After the first cycle, five similar cycles were performed over the same catalyst sample. It is important to note that no CO emission was detected during the DPM oxidation cycles.

To determine the catalytic effect, an uncatalyzed particle matter oxidation cycle was performed under the same conditions over quartz wool from 25 to 800 °C.

3. Results and discussion

3.1. Characterization of the diesel particulate matter and diesel exhaust of the vessel

The FT-IR spectrum of the DPM used in this investigation is shown in Fig. 2. Principal characteristic peaks revealed in the spectrum corresponds to the C—H asymmetric and symmetric stretching of aliphatic groups at 2953 cm^{-1}, 2923 cm^{-1} and 2853 cm^{-1}; C—O stretching of carbonyl groups at 1700 cm^{-1}; C=C stretching of aromatics and alkenes at 1560 cm^{-1}; and aliphatic C—H plane deformation of CH_2/CH_3 groups at 1450 cm^{-1} and 1380 cm^{-1} [21,22]. The experiment was performed in triplicate. Similar qualitative results were obtained for the 3 DPM spectra. The amounts of DPM retained by the catalysts during 3 deposition cycles are summarized in Table 1. While the amounts of DPM deposited over a particular catalyst during 3 burning cycles are

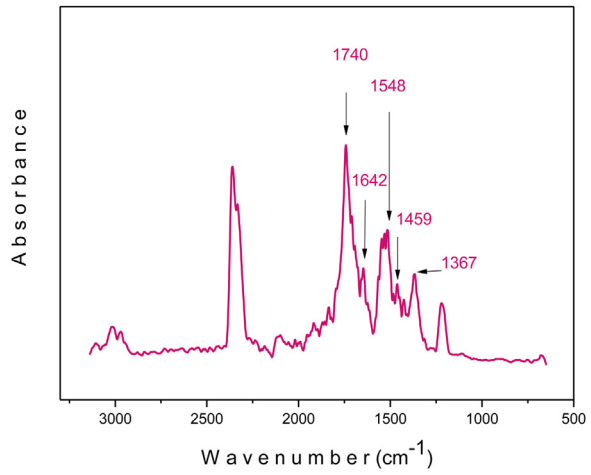

Fig. 2. FTIR spectrum of diesel particulate matter sampled from the combustion vessel exhaust.

similar, the similarity in the values of DPM quantities for different catalysts suggests the catalysts have similar capacities to retain DPM.

The results obtained from the qualitative analysis performed by FT-IR spectroscopy of the emitted gases from the diesel burning vessel exhaust are summarized in Table 2. As can be seen, the concentration of sulfur compounds in the exhaust gas is very low (e.g. $[SO]_2$ = 15 ppm).

3.2. Catalysts characterization

3.2.1. Surface area analysis

Table 3 summarizes BET surface areas of the freshly prepared silver-supported catalysts and after using them in 6 DPM oxidation

Table 1
Amounts of DPM deposited on the catalysts during diesel combustion in the vessel.

Catalyst	Diesel particulate matter (mg)		
	1st	2nd	3rd
SiO_2	8.55	8.43	8.74
ZnO	8.66	8.35	8.55
3%Ag/SiO_2	8.31	8.59	8.63
3%Ag/ZnO	8.36	8.30	8.48

Table 2
Diesel emissions (from the burning vessel) composition.

Compound	Concentration(ppmV)	Compound	Concentration(ppmV)
Allene	122	1,2-epoxybutane	532
Butane	41	Ethylene oxide	53
Ethylene	27	Hydrogen peroxide	34
Methane	16	Maleic anhydride	19
Propyne	122	Acetic acid	24
Isoprene	17	Propionic acid	18
2-methyl-2-butene	151	Crotonaldehyde	46
3methyl-1-butene	86	Acetophenone	12
n-pentane	20	Cyclohexanone	2890
2-pentene	47	Methyl vinil ketone	1017
Alpha-pinene	480	Benzyl alcohol	9
Beta-pinene	36	n-butil alcohol	26
Cyclohexene	23	Ethanol	11
Dicyclopentadiene	514	2-ethoxy ethanol	19
n-hexane	32	Isopropanol	112
1-hexene	55	1-nonanol	79
2-methypentane	19	n-propanol	76
3-methylpentane	19	Ethyl butyrate	516
2-methyl-1-pentene	41	Chloromethyl methyl ether	7
2-methyl-2-pentene	31	Nitric oxide	13
1-nonene	64	Acrylo nitrile	56
Isopropyl benzene	14	Methyl amine	700
Mesitylene	49	Nitro benzene	126
Naphthalene	21	Ethyl mercaptane	340
n-propyl benzene	210	Sulfur dioxide	11
Ter-bulyl benzene	186	Tetrehydrothiophene	49
1,2,3, trimethyl benzene	394	Thiophene	193
m-xylene	68	Carbon tetrachloride	48
Arsine	760	Iodomethane	50
Hydrogen bromide	19	Chloroethane	82
Phosphine	251	1,1-dichloroethane	106
Silane	191	1,1,2,2,-tetrachloroethane	101
Carbon dioxide	53824	m-dichlorobenzene	121
Carbon monoxide	2072	o-dichlorobenzene	63
Chlorine dioxide	146	p-dichlorobenzene	138

Table 3
Characteristics of the catalytic samples used in this study.

Catalyst	Specific surface area (m^2g^{-1})	
	Fresh sample	After oxidation cycles
SiO_2	180	159
3%Ag/SiO_2	156	153
ZnO	40	35
3%Ag/ZnO	34	30

cycles. It can be seen that the addition of Ag results in a decrease in surface area of both SiO_2 and ZnO supports. After 6 DPM oxidation cycles, an additional drop in surface area is observed for both the catalysts.

3.2.2. X-ray diffraction characterization of the catalysts

XRD spectra of the fresh SiO_2 and 3%Ag/SiO_2 samples are shown in Fig. 3. The 3%Ag/SiO_2 sample revealed four clear diffraction peaks of metallic Ag (JCPDS # 87-0717) around $2\theta = 38°$, 44°, 64°, 78°, which correspond to the (111), (200), (220), and (311) planes of face-centered cubic structures of silver, along with a weak peak associated to cubic Ag_2O ($2\theta = 32°$). The result indicates that a high amount of metallic silver (Ag^0) is present in the catalyst. Fig. 4 shows the XRD spectra of freshly prepared 3%Ag/ZnO and ZnO samples. The 3%Ag/ZnO spectrum revealed the characteristic bands of Ag^0 ($2\theta = 38°$, 44°, 64°), and Ag_2O ($2\theta = 32°$), along with the diffraction peaks of ZnO ($2\theta = 32°$, 34°, 36°, 47°, 56°, 63°, 66°, 68°, and 69°) in hexagonal wurtzite phase (JCPDS # 36-1451). The results suggest that despite the use of strong reduction conditions during catalyst preparation, in both the samples, a part of the deposited Ag was not reduced to Ag^0.

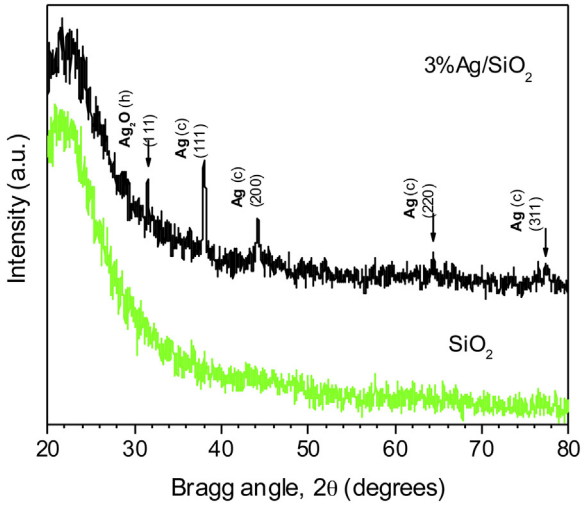

Fig. 3. XRD spectra of fresh 3%Ag/SiO_2 and fresh SiO_2.

3.2.3. TEM study of the catalysts

Representative TEM images of 3%Ag/SiO_2 and 3%Ag/ZnO catalysts before and after the DPM oxidation cycles are presented in Fig. 5. The Ag particles can be seen as dark contrasts on the surface of the supports particles. The images revealed no traces of carbon or other particle matter after 6 DPM oxidation cycles.

3%Ag/SiO_2

From Fig. 5, we can see the formation of well-dispersed Ag nanoparticles of uniform sizes, with average size (c.a.) 3.03 nm over the fresh catalyst. After its use in oxidation cycles, the Ag nanopar-

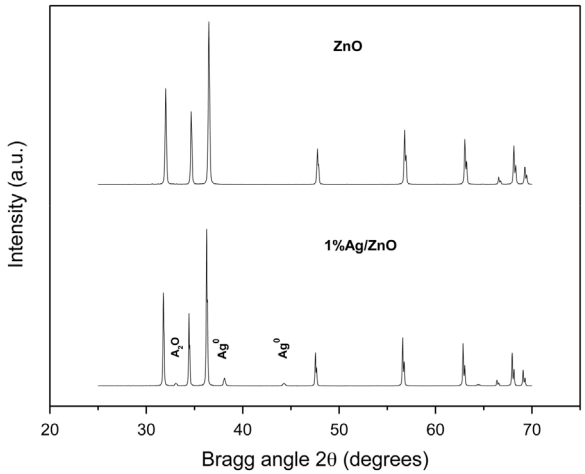

Fig. 4. XRD spectra of fresh ZnO and fresh 3%Ag/ZnO.

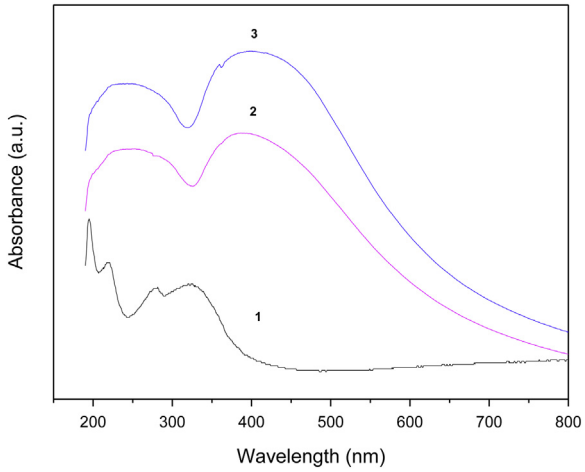

Fig. 6. Absorption spectra of: 1) fresh SiO_2; 2) 3%Ag/SiO_2 before DPM oxidation cycles; 3) 3%Ag/SiO_2 after DPM oxidation cycles.

ticles aggregated to some extent, forming Ag particles of (c.a.) 5.36 nm average size. The increase of average size of Ag particles due to the high temperature catalytic process is about 1.77 times (77%). It is interesting noting that, even after the catalytic cycles, the average size of the Ag nanoparticles in silica matrix remains close to 5.0 nm, which is ideal for their catalytic applications.

3%Ag/ZnO

Formation of well dispersed Ag nanoparticles of 3.0–11.4 nm size range, with average size of (c.a.) 6.36 nm can be seen for the fresh 3%Ag/ZnO catalyst (Fig. 5). However, after the DPM oxidation cycles, the Ag nanoparticles agglomerated due to high temperature, forming only a very few bigger Ag NPs of average size (c.a.) 88.0 nm. The increase of average size due to high temperature catalytic processes is about 13.84 times (1284%).

3.2.4. Diffuse reflectance spectra of the catalysts

3%Ag/SiO_2

The UV–vis diffuse reflectance spectra (DRS) of SiO_2 and 3%Ag/SiO_2 before and after their use in DPM oxidation, were recorded in absorption mode and presented in Fig. 6. The absorption spectrum of 3%Ag/SiO_2 before its use in DPM oxidation

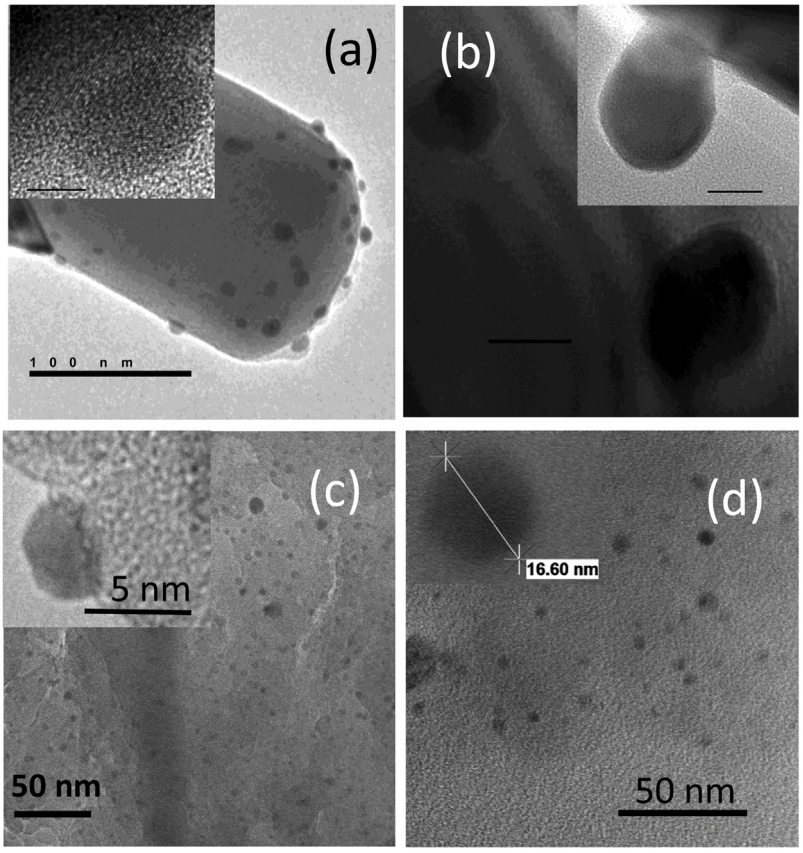

Fig. 5. Typical TEM images of the a) unused Ag/ZnO, b) used Ag/ZnO, c) unused Ag/SiO_2, and d) used Ag/SiO_2 catalysts. Magnified images of typical Ag particles in the samples are presented as corresponding insets.

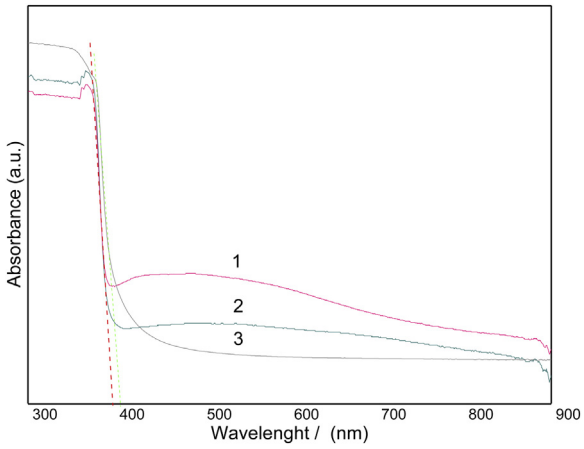

Fig. 7. Absorption spectra of: 1): 3%Ag/ZnO before DPM oxidation cycles; 2): 3%Ag/ZnO after DPM oxidation cycles; 3) fresh ZnO.

revealed two bands (spectrum 2). The first band, spreading through 320 and 600 nm, with maximum around 400 nm, corresponds to the overlapping of silver surface plasmon resonance (SPR) signal (400–550 nm) with the σ- σ* and n- σ* transition signals of Ag_n clusters, which appear in the 330–360 nm and 440–540 nm spectral range, respectively [23,24]. The absorption band appearing around 400 nm was suggested [25] to be the SPR band of metallic Ag particles, attributed to the collective oscillations of the conduction band electrons, induced by the incident electromagnetic radiation [26]. The second band at around 270 nm has been attributed to Ag_4^{2+} [27,28]. As can be seen in this figure, the absorption spectrum of 3%Ag/SiO_2 after its use in oxidation cycles (spectrum 3) presents the same bands as the catalyst before using it in oxidation cycles (spectrum 2). The result suggests that the same electronic states of silver prevail in 3%Ag/SiO_2 even after six DPM oxidation cycles.

3%Ag/ZnO

The absorption spectra of ZnO and 3%Ag/ZnO before and after their use in DPM oxidation cycles are represented in Fig. 7. The absorption spectrum of the fresh 3%Ag/ZnO catalyst (spectrum 1) revealed two bands. The first band appeared between 400 and 650 nm with maximum around 450 nm, which corresponds to the characteristic surface plasmon resonance (SPR) band of silver nanoparticles [26,29]. The second band is observed with onset at around 400 nm, which is close to the absorption edge of ZnO [30], showing a band gap value around 3.1 eV. Spectrum 2, corresponding to the diffuse reflectance spectrum of 3%Ag/ZnO after its use in DPM oxidation cycles, revealed that the intensity of the absorption band between 400 and 600 nm reduces considerably after using the catalyst in DPM oxidation cycles, along with a shift towards higher wavelengths, suggesting probably an electron deficit of the Ag nanoparticles, and size increase during DPM oxidation at high temperature. However, the intensity and position of the second band, corresponding to the absorption edge of ZnO (at around 400 nm) remained the same for both samples.

As can be noticed from Fig. 7, while the absorption edge of pure ZnO (spectrum 3) resides around 400 nm (corresponding to a band gap around 2.9 eV), its absorption edge in the 3%Ag/ZnO catalyst (freshly prepared and after DPM cycles) is located around 390 nm. Such a blue-shift of the absorption edge in the composite catalyst might had been occurred due to an interfacial electronic transfer from Ag nanoparticles to ZnO support. Such an electron transfer process would result in a deficit of electrons at the surface of Ag nanoparticles and an enrichment of electrons in ZnO support, leading to the blue shift of the excitonic absorption band of ZnO, effectively increasing its band gap energy.

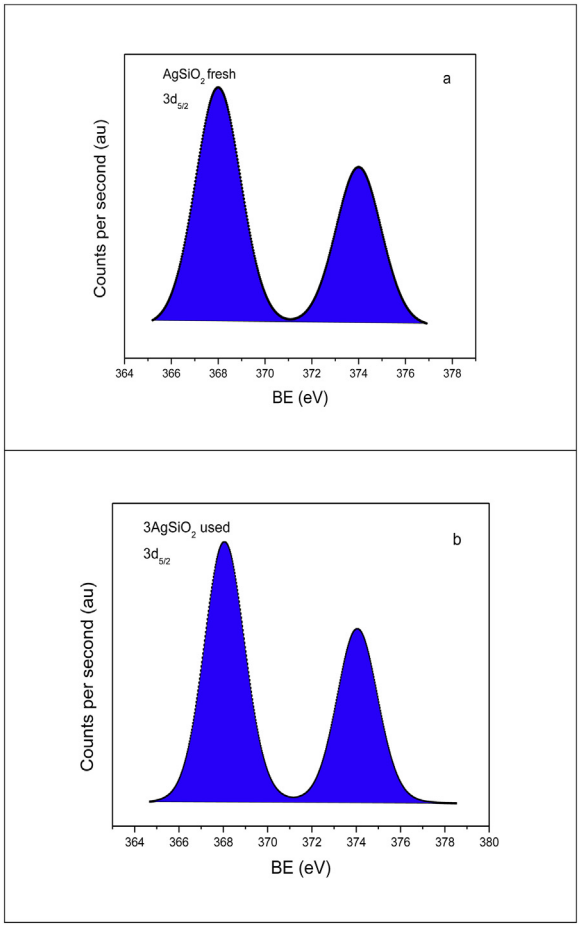

Fig. 8. XPS spectra of 3%Ag/SiO_2: (a) before, and (b) after 6 DPM oxidation cycles.

3.2.5. XPS characterization of the catalysts

The activity of a catalyst in oxidation reactions is closely associated to its capability to activate oxygen. To determine the possible interactions between the catalysts and oxygen, the electronic states of Ag supported over SiO_2 and over ZnO were determined by XPS before and after using the catalysts in the DPM oxidation cycles.

3%Ag/SiO_2

The XPS spectra of the freshly prepared 3%Ag/SiO_2 catalyst and after its use in DPM oxidation are presented in Fig. 8. As can be seen, the freshly prepared sample revealed well defined single component Ag $3d_{5/2}$ emission band peaked around 368.0 eV, corresponding to Ag^0 electronic state [31–33]. The XPS spectrum of the sample revealed very similar Ag $3d_{5/2}$ emission after its utilization in six DPM oxidation cycles (Fig. 10, Table 4). The position (binding energy) of Ag $3d_{5/2}$ emission remained the same as that of the unused catalyst, suggesting that the zero valent (metallic) electronic state of silver in 3%Ag/SiO_2 remained unaltered, thus the oxidized Ag^+ species were not formed, despite the strong high temperature oxidation conditions to perform the DPM oxidation cycles. The high stability of Ag^0 can be explained considering the very low enthalpy of formation of bulk Ag_2O (- ΔH_f = 7 kcal/mol) [34]. This value indicates that the surface oxidation of Ag^0 to Ag_2O is improbable, even in high temperature oxidation conditions.

It is worth noting that the XRD spectrum of 3%Ag/SiO_2 (Fig. 3) revealed a weak peak associated to Ag_2O in cubic phase, indicating the presence of a fraction of silver in Ag^+ state. These apparent contradictions between the XRD and XPS results, can be justified considering that the XRD technique is a bulk technique, providing information of the entire sample, while XPS technique is a surface

Table 4
Binding energy position of the components, and Ag/Si or Ag/Zn atomic ratios at the surface of the fresh catalysts (before) and after their use in six DPM oxidation cycles. The% peak area of Ag $3d_{5/2}$ components is presented in parentheses.

Catalyst	Ag $3d_{5/2}$ (eV)		Si $2p_{3/2}$ (eV)	Zn $2p_{3/2}$ (eV)	Atomic ratio	
					Ag/Si	Ag/Zn
3%Ag/SiO_2, fresh	368.0	(100)	103.8		0.05	
3%Ag/SiO_2, used	367.9	(100)	103.7		0.04	
3%Ag/ZnO, fresh	367.3	(80)		1021.7		0,26
	368.3	(20)				
3%Ag/ZnO, used	367.2	(91)		1021.7		0.17
	368.4	(9)				

technique, providing surface composition of the catalyst, detecting the presence of metallic Ag^0 species at its surface.

The XPS estimated Ag/Si atomic ratios in the catalyst before and after its use in DPM oxidation cycles are presented in Table 4. The Ag/Si atomic ratio at the surface of the catalyst before (0.05) and after its use in DPM oxidation cycles (0.04) remained rather the same. The results suggest that the Ag particles size was not altered by the high temperature DPM oxidation cycles. This suggestion is supported by the micrographs obtained from TEM which show only a slight increase of Ag particles after the reaction cycles (Fig. 5).

3%Ag/ZnO

To examine the oxidation state of silver in 3%Ag/ZnO, XPS analysis was performed before and after its use in six DPM oxidation cycles. Binding energies for the core electrons of the catalysts are reported in Table 4.

The XPS spectrum of 3%Ag/ZnO catalyst before its use in DPM oxidation is displayed in Fig. 9, where we can observe the Ag $3d_{5/2}$ emission band with two components, located around 367.3 and 368.3 eV, corresponding to Ag^{1+}, and Ag^0 electronic states, respectively [31–33,35,36]. The XPS spectrum of the sample after its use in DPM oxidation cycles (Fig. 9b) revealed the Ag $3d_{5/2}$ emission band with the same two components around 367.2 and 368.4 eV, corresponding to Ag^{1+}, and Ag^0 electronic states, respectively. However, their relative intensity changed. The relative content of silver in Ag^0 state decreased from 20% to 9%, and the relative content of Ag^{1+} increased from 80% to 91%, indicating that during oxidation cycles, a fraction of silver in Ag^0 state transformed to Ag^{1+} state. Now, the oxidation of Ag^0 to Ag^{1+} is not favored under the used reaction conditions, as we discussed to explain the high stability of Ag^0 in 3%Ag/SiO_2.

3.2.6. TEM analysis of the catalysts

The TEM image of the fresh 3%Ag/ZnO sample (Fig. 5) shows formation of small, highly dispersed Ag nanoparticles over ZnO surface. It is well known that small metal nanoparticles can present electron deficiencies due to metal-support interactions [37,38] in contrary to that of larger metal nanoparticles. This fact could explain the high relative content of Ag^+ species at the surface of ZnO in the fresh 3%Ag/ZnO catalyst. However, the TEM study shows that after using the catalyst in DPM oxidation cycles, the size of the Ag nanoparticles increases drastically (1284%). While such increase in particles size of Ag clusters reduces the contact surface area of Ag-ZnO interface, it also reduces the probability of electron transfer from Ag to ZnO support. In other words, the increase of Ag nanoparticle size would increase the relative content of Ag^0 at the ZnO surface. Notwithstanding, our XPS results revealed an increase in the relative content of Ag^+ in the 3%Ag/ZnO catalyst after using in DPM cycles.

To explain these apparent opposite results, we must consider the effect of ZnO semiconductor in 3%Ag/ZnO composite and the concept of energy level alignment between Ag nanoparticles and ZnO support. The high content of Ag^{1+} at the catalyst surface might

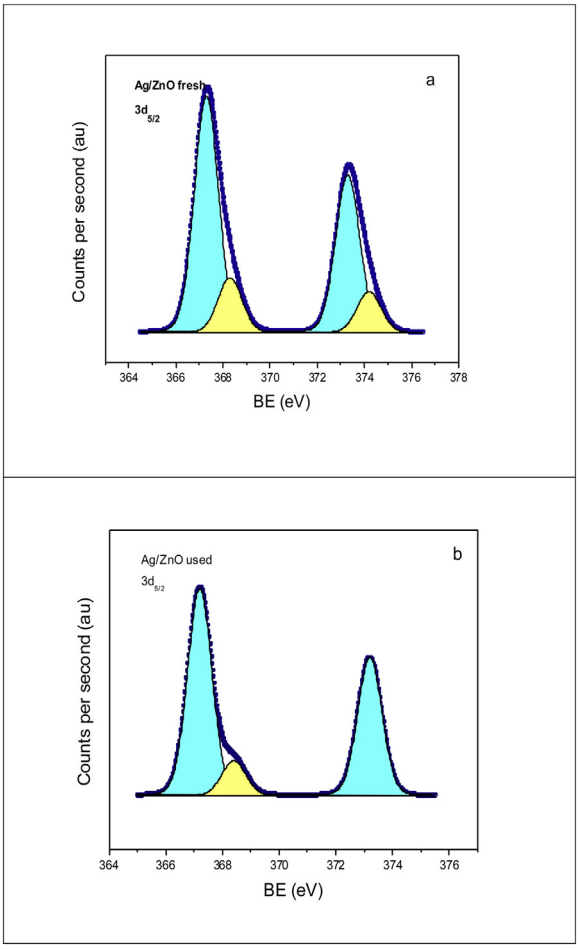

Fig. 9. XPS spectra of 3%Ag/ZnO: (a) before, and (b) after 6 DPM oxidation cycles.

had been caused by the electron transfer from Ag^0 to ZnO particles during the formation of ZnO-Ag composite [39]. It is well known that the work function of ZnO (~4.5 eV) is larger than that of Ag (4.26 eV). The Fermi energy level of Ag resides at higher level than that of ZnO due to its smaller work function; implying that the electrons will migrate from silver to the conduction band (CB) of ZnO to achieve the Fermi level equilibration when they are in contact, decreasing the stability of metallic silver at the metal-support interface [40,41]. The electron transfer from Ag to ZnO results in the formation of Ag^{1+}, as revealed by XPS analysis. These assumptions are in agreement with the results obtained from the absorption spectra of the 3%Ag/ZnO before and after the DPM oxidation cycles presented in Fig. 7. The decrease of the intensity of metallic Ag after the DPM oxidation cycles might be due to the decrease of Ag^0 metallic species, resulting in a decrease in intensity of the SPR band, which is red-shifted [42]. Consequently, this transfer might result

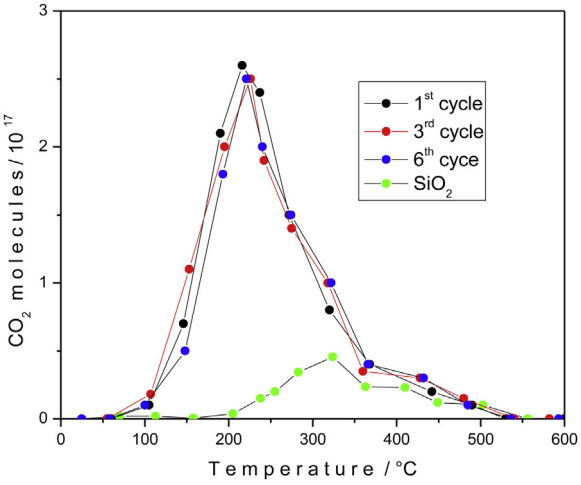

Fig. 10. Evolution of CO_2 as a function of temperature during DPM oxidation over 3%Ag/SiO_2.

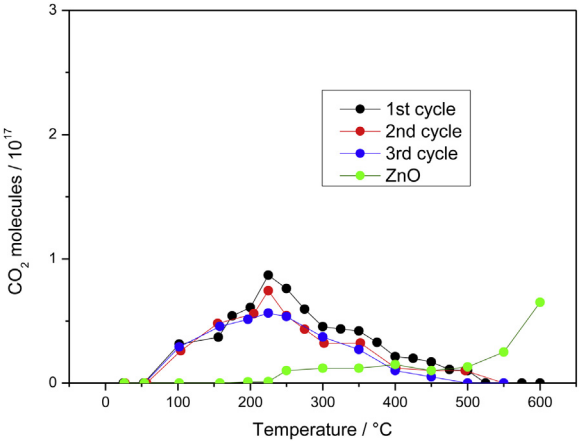

Fig. 11. Evolution of CO_2 as a function of temperature during DPM oxidation over 3%Ag/ZnO.

in an enrichment of electrons in ZnO support, resulting in a blue shift of its absorption band edge.

3.3. Diesel particulate matter oxidation over the catalysts

In order to compare the activities of the different catalysts, the results obtained on the CO_2 evolution during the DPM oxidation cycles (6 oxidation cycles) as a function of temperature are presented in Figs. 10 and 11. The values calculated from these figures, led to the construction of Table 5, which summarizes the integrated areas under CO_2 evolution curves during particulate matter oxidation over the catalysts (intensity of CO_2 evolution) ($[CO_2]_{Cat}$); the temperatures at which the oxidation started ($T_{Initial}$); the temperatures when the oxidation reached a maximum (T_{Max}) and the temperatures when the reaction completes (T_{Final}).

Diesel particulate matter oxidation over SiO_2

The evolution of the DPM oxidation over SiO_2 at temperatures between 25 and 600 °C (Fig. 10) revealed the production of very small amounts of CO_2 during the 1st oxidation cycle. The amounts of generated CO_2 remained rather constant during the subsequent cycles as reported in Table 5.

Diesel particulate matter oxidation over 3%Ag/SiO_2

Fig. 10 shows of CO_2 evolution, as a function of the oxidation temperature, during 6 particulate matter oxidation cycles over the 3%Ag/SiO_2 catalyst. In all the six CO_2 evolution curves, there appeared a broad signal through 150–300 °C, peaking at about 220 °C, indicating that the highest DPM oxidation temperature (T_{Max}) remains the same from cycle to cycle. The unaltered position of T_{Max} would mean that during 6 oxidation cycles, the stoichiometry and electronic structure of the catalyst remained the same. Now, XPS results revealed that the surface metallic electronic state of silver in the catalyst remained the same after six DPM oxidation cycles. The constant activity during DPM oxidation cycles and unaltered electronic state of Ag, suggest that metallic Ag^0 is the active species for the reaction. The results presented above indicate that this catalyst is thermally stable and could operate at the temperatures of diesel engine exhaust gases.

Table 5
Integrated areas under CO_2 evolution, starting temperatures of oxidation ($T_{Initial}$); temperatures of maximum oxidation (T_{Max}), and the temperatures of reaction completion (T_{Final}) for the catalysts during DPM oxidation cycles.

Catalyst	Cycle	Intensity of CO_2 evolution (10^{18} molecules)	Temperatures (°C)		
			$T_{Initial}$	T_{Max}	T_{Final}
Quartz wool		450	477	726	820
SiO_2	1st	72	200	330	550
	2nd	69	210	345	550
	6th	74	220	350	550
ZnO	1st	64	225	–	–
	2nd	55	256	–	–
	6th	48	248	–	–
3%Ag/SiO_2	1st	354	70	220	542
	2nd	346	105	225	540
	6th	353	100	223	536
3%Ag/ZnO	1st	146	102	228	475
	2nd	132	104	228	450
	6th	130	102	230	450

Diesel particulate matter oxidation over ZnO

The evolution of the DPM oxidation over ZnO at temperatures between 25 and 600 °C during the 1st cycle is presented in Fig. 11. This result revealed the production of very small amounts of CO_2 during DPM oxidation; which is even lower than the amount of CO_2 generated during the 1st DPM oxidation cycle performed using SiO_2. During the subsequent 5 DPM oxidation cycles (Table 5), the amounts of generated CO_2 remained very low.

These results suggest that, although the DPM quantities deposited over SiO_2 and ZnO are similar (Table 1; 8.55 mg and 8.66 mg, respectively), their oxidation activities are different.

Diesel particulate matter oxidation over 3%Ag/ZnO

Fig. 11 shows the temperature evolution of CO_2 during 6 particulate matter oxidation cycles over the 3%Ag/ZnO. As can be seen, during the first oxidation cycle, there appeared a small CO_2 signal at about 225 °C (T_{Max}). This signal decreased slightly during the successive cycles, indicating a slight deactivation of the catalyst. Now, the results obtained from the DRS and XPS analyses of the catalyst revealed that after the oxidation cycles, the content of Ag^0 decreased; which suggests that there is a direct dependence on the oxidation activity and the percentage of Ag^0 on the 3%Ag/ZnO catalyst surface.

Catalysts diesel burning efficiency

To estimate the catalytic activity of the different catalyst, the CO_2 evolution during the oxidation of DPM deposited on quartz wool was also monitored. The results presented in Table 5 indicate that DPM oxidation initiated at about 477 °C ($T_{Initial}$), and competed around 820 °C (T_{Final}). The T_{Max} detected was about 726 °C. The result permitted to calculate the total area under the CO_2 evolution curve between 25 and 820 °C. This value is considered as a measure of the total amount of carbon in the particulate matter, generated from the exhaust gas of the vessel and accumulated

Table 6
CO_2 evolution, and estimated efficiency of the 3%Ag/SiO_2 and 3%Ag/ZnO catalysts for the 1st, 2nd, and 6th oxidation cycles of DPM oxidation. Temperature range: 25–600 °C.

Catalyst	Intensity of CO_2 evolution (10^{18} molecules)			Catalyst efficiency		
	1st	2nd	6th	1st	2nd	6th
Quartz wool*	450					
SiO_2	72	69	74	0.16	0.15	0.16
ZnO	24	19	15	0.05	0.00	0.00
3%Ag/SiO_2	354	346	358	0.78	0.76	0.82
3%Ag/ZnO	146	132	130	0.32	0.29	0.28

* Temperature range: 25–820 °C.

for 1 h ($[CO_2]_{Ref}$). To estimate and compare the catalytic activity of the catalysts studied in this investigation, we define the Relative Catalytic Activity of the catalyst as the ratio of CO_2 concentration evolved during the catalytic process and the same in absence of the catalyst (using only quartz wool) as:

$$Relative\ \ Catalytic\ \ Activity = \frac{[CO_2]_{Cat}}{[CO_2]_{Ref}},$$

where $[CO_2]_{Cat}$ is the area under CO_2 evolution curve (between 25 °C and 600 °C) during DPM oxidation over the catalyst, and $[CO_2]_{Ref}$ is the area under CO_2 evolution curve during DPM oxidation over quartz wool. The $[CO_2]_{Cat}$ and calculated Relative Catalytic Efficiency values for the catalysts for different oxidation cycles have been presented in Table 6. As can be seen from this table, the 3%Ag/SiO_2 catalysts is far more efficient than 3%Ag/ZnO, and remains highly active during six DPM oxidation cycles.

3.4. Mechanistic considerations of DPM oxidation over the catalysts

It is well known that metallic silver is an oxidation catalyst which can form several sub-oxide species (oxygen admolecule, superoxide ion, subsurface oxygen, oxygen adatoms, and oxidic oxygen adatoms) in oxidation atmosphere [43–48]. Nakatsuji et al. [49,50] studied the mechanism of silver catalyzed partial oxidation by theoretical calculations and concluded that the active species was superoxide ion O_2^- which was molecularly adsorbed. Other investigations have also demonstrated that Ag^0 promotes the formation of superoxide ions [51–55]. Annegi et al. pointed out that the superoxide ions generated by metallic silver might assist carbon oxidation [19].

The results presented in this investigation suggest that Ag^0 species present in 3%Ag/SiO_2 and 3%Ag/ZnO might be responsible for DPM oxidation. Based on the results presented in the previous reported studies, in which the presence of superoxide ions O_2^- was demonstrated [49–55], we propose the following probable mechanism in terms of Eley-Rideal reaction pathways to explain the activity of the catalysts studied for DPM oxidation.

1. Adsorption of O_2 on the Ag^0 catalytic sites.
2. Generation of superoxide species O_2^- by the transfer of one electron from Ag^0 to the moleculary adsorbed O_2 as proposed by Nakatsuji et al. [49,50] to describe the mechanism of metallic-silver catalyzed ethylene epoxidation.
3. Reaction of the DPM particle with the adsorbed superoxide molecule on Ag^0.
4. Reaction of C—H and/or C=C bonds present in the DPM particle with the O_2^- formed at Ag^0[19].

The superoxides formed on Ag^0 would have strongly increasd the probability of DPM oxidation, resulting in the production of CO_2 and H_2O molecules as final products.

Now, it is well known that Ag^{1+} is not active in oxidation reactions, thus it is not active in DPM oxidation. The very low activity of 3%Ag/ZnO for DPM oxidation can be explained considering the high content of Ag^{1+} species present at the catalyst surface, therefore, the low content of Ag^3 which might have generated very low amounts of superoxides (O_2^-), resulting in very low activity for DPM oxidation (Fig. 11).

In 3%Ag/SiO_2, electronic transfer from Ag^0 to SiO_2 does not takes place due to the insulating character of SiO_2. However, in 3%Ag/ZnO, due to favorable electronic structure at the metal-semiconductor interface, electrons from Ag^0 move to the conduction band of ZnO, producing Ag^{1+} at the surface of ZnO. During DPM oxidation cycles, this electron transfer process enhances, reducing the oxidation capacity of Ag/ZnO. The high content of metallic Ag^0, stabilized at the surface of SiO_2 results in a very high activity for DPM oxidation (Fig. 10).

4. Conclusions

In summary, the results obtained in this investigation suggest that catalytic activity of Ag supported metal oxide catalysts for DPM oxidation is a function of the electronic state of Ag at their surfaces, which depends on the electronic interactions of Ag and the support, especially on the work function values of Ag and the support.

The high diesel particulate matter oxidation activity presented by 3%Ag/SiO_2 may be due to the very high amount of metallic Ag^0 at the surface, stabilized due to the lack of electronic interactions between Ag and SiO_2 (insulator). The presence of Ag^0, at the surface of the composite catalysts, generates high amounts of O_2^-, the very active species for improving diesel particulate matter oxidation. However, the electronic interactions of Ag with ZnO (n-type semiconductor) at the metal-support interface led to the formation and stabilization of high amounts of Ag^{1+} species, which are inactive for the O_2^- generation over 3%Ag/ZnO surface, resulting in a very low activity for diesel particulate matter oxidation.

Acknowledgements

Financial support from the Secretaria de Energía-Consejo Nacional de Ciencia y Tecnología (SENER-CONACYT) is gratefully acknowledge (Cluster Biodiesel Avanzado Proyecto 250014).The authors acknowledge Vicerrectoría de Investigación y Estudios de Posgrado (Proyectos 2017) and Dirección de Innovación y Transferencia de Conocimiento (Proyectos 2017) of the Benemérita Universidad Autónoma de Puebla, México, for their financial supports.The authors acknowledge M.C. Felipe Barffuson Dominguez and M.C. Roberto Mora Monroy, Department of Physics, Universidad de Sonora, Mexico, for the helps in acquiring TEM data and XPS spectra of the catalysts.

References

[1] A. Bueno-Lopez, Appl. Catal. B 146 (2014) 1–11.
[2] K. Krishna, A. Bueno-Lopez, M. Makkee, J.A. Moulijn, Appl. Catal. B 75 (2007) 189–200.
[3] J. Zokoe, P.J. McGinn, Chem. Eng. J. 262 (2015) 68–77.

[4] I. Atribak, A. Bueno-López, A. García-García, Combust. Flame 157 (2010) 2086–2094.
[5] D. Fino, V. Specchia, Powder Technol. 180 (2008) 64–73.
[6] G. Lepperhoff, H. Luders, P. Barthe, J. Lemaire, SAE Paper, 1995 (950369).
[7] K. Hinot, H. Burtscher, A.P. Weber, G. Kasper, Appl. Catal. B 71 (2007) 271.
[8] R. Allansson, P. Blakeman, B. Cooper, H. Hess, P.J. Silcock, A.R. Walker, SAE Technical Paper, 2002 (2002-01-0428).
[9] A. Setiabudi, B.A.A.L. v. Setten, M. Makkee, J.A. Moulijn, Appl. Catal. B 35 (2002) 159–166.
[10] D. Reichert, T. Finke, N. Atanassova, H. Bockhorn, S. Kureti, Appl. Catal. B 84 (2008) 803.
[11] M. Sun, L. Wang, B. Feng, Z. Zhang, G. Lu, Y. Guo, Catal. Today 175 (2011) 100–105.
[12] L.L. Hueso, A. Caballero, M. Ocaña, A.R. Gonzalez-Elipe, J. Catal. 257 (2008) 334–344.
[13] I. Atribak, A. Bueno-Lopez, A. Garcia-Garcia, P. Navarro, D. Frias, M. Montes, Appl. Catal. B 93 (2010) 267–273.
[14] N. Zouaoui, M. Issa, D. Kehrli, M. Jeguirim, Catal. Today 189 (2012) 65–69.
[15] J. Liu, Z. Zhao, C. Xu, A. Duan, Appl. Catal. B 78 (2008) 61–72.
[16] K. Yamasaki, Y. Sakakibara, F. Dong, H. Shinjoh, Appl. Catal. A 476 (2014) 113–120.
[17] C. Lee, J. Park, Y. Shul, H. Einaga, Y. Teraoka, Appl. Catal. B 174 (2015) 185–192.
[18] S. Liu, X. Wu, W. Liu, W. Chen, R. Ran, M. Li, D. Weng, J. Catal. 337 (2016) 188–198.
[19] E. Aneggi, J. Lorca, C. de Leitenburg, G. Dolcetti, A. Trovarelli, Appl. Catal. B 91 (2009) 489–498.
[20] G. Corro, U. Pal, E. Ayala, E. Vidal, E. Guilleminot, Top. Catal. 56 (2013) 467–472.
[21] M. Salamanca, F. Mondragon J.R., P. Agudelo, P. Benjumea, A. Santamaria, Combust. Flame 159 (2012) 1100–1108.
[22] L.J. Bellamy, The Infrared Spectra of Complex Molecules, Chapman and Hall, London, 1975.
[23] G.A. Ozin, H. Huber, Inorg. Chem. 17 (1879) 155–159.
[24] S.A. Michell, G.A. Kenney-Wallace, G.A. Ozin, J. Am. Chem. Soc. 123 (1983) 6030–6033.
[25] N.E. Bogdanchikova, M.N. Dulin, A.V. Toktarev, G.B. Shevnina, V.N. Kolomiichuk, V.I. Zaikovskii, V.P. Petranovskii, Stud. Surf. Sci. Catal. 84 (1994) 1067.
[26] M. Ziyad, S. Arsalane, M. Kacimi, G. Coudurier, J.M. Millet, J.C. Vedrine, Appl. Catal. 147 (1996) 363.
[27] T. Linnert, P. Mulvaney, A. Henglein, H. Weller, J. Am. Chem. Soc. 112 (1990) 4657.
[28] B.G. Ershov, E. Janata, A. Henglein, J. Phys. Chem. 97 (1993) 867.
[29] H. Liu, Y. Hu, Z. Zhang, X. Liu, H. Jia, B.V. Xu, Appl. Surf. Sci. 355 (2015) 644–652.
[30] Y. Hu, H.J. Chen, J. Nanopart. Res. 10 (2008) 401–407.
[31] M. Richter, M. Langpape, S. Kolf, G. Grubert, R. Eckelt, J. Radnik, M. Schneider, M.M. Pohl, R. Fricke, Appl. Catal. B 36 (2002) 261.
[32] G.B. Hoflund, Z.F. Hazos, Phys. Rev. B 62 (2000) 11126.
[33] X. She, M. Flytzani-Stephanopoulos, J. Catal 237 (2006) 79–93.
[34] D.E. Fein, I.E. Wachs, J. Catal. 210 (2002) 241.
[35] W.W. Lu, S.Y. Gao, J.J. Wang, J. Phys. Chem. C 112 (2008) 16792–16800.
[36] S. Balachandran, K. Selvam, B. Babub, M. Swaminathan, Dalton Trans. 42 (2013) 16365–16374.
[37] M. Ahmadi, H. Mistry, B. Roldan Cuenya, J. Phys. Chem. Lett. 7 (2016) 3519–3533.
[38] M. Cargnello, V.V.T. Doan-Nguyen, T.R. Gordon, R.E. Diaz, E.A. Stach, R.J. Gorte, P. Fornasiero, C.B. Murray, Science 341 (2013) 771–773.
[39] F. Shwun, C. Xu, Z. Jin, J. Guo, S. Fang, Z. Shi, J. Wang, J. Phys. Chem. C 117 (2013) 18627–18633.
[40] D.D. Lin, H. Wu, R. Zhang, W. Pan, Chem. Mater. 21 (2009) 3479–3484.
[41] Z. Han, L. Ren, Z. Cui, C. Chen, H. J. Chen Pan, Appl. Catal. B 126 (2012) 298–305.
[42] M.K. Lee, T.G. Kim, W. Kim, Y.M. Sung, J. Phys. Chem. C 112 (2008) 10079–10085.
[43] Lj. Kundakovic, M. Flytzani-Stephanopolus, Appl. Catal. A 183 (1999) 35.
[44] A. Nagy, G. Mestl, Appl. Catal. A 188 (1999) 337.
[45] Z. Qu, M. Cheng, W. Huang, X. Bao, J. Catal. 229 (2005) 446.
[46] N. Gungor, S. Gunister, W. Mista, H. Teterycz, R. Klimkiewicz, Appl. Clay Sci. 32 (2006) 291.
[47] Z. Qu, M. Chen, X. Dong, X. Bao, Catal. Today 93-95 (2004) 247.
[48] G.I.N. Waterhouse, G.A. Bowmaker, J.B. Metson, Appl. Surf. Sci. 214 (2003) 36.
[49] H. Nakatsuji, Z.M. Hu, H. Nakai, Int. J. Quant. Chem. 65 (1997) 839–855.
[50] H. Nakatsuji, Int. J. Quant. Chem. 42 (1992) 725.
[51] D.E. Fein, I.E. Wachs, J. Catal. 210 (2002) 241.
[52] R.B. Clarkson, J. Catal. 33 (1974) 392.
[53] A. Aboukais, M. Jarjoui, J.C. Verdrine, P.C. Gravelle, J. Catal. 47 (1977).
[54] S. Tanaka, T. Yamashina, J. Catal. 40 (1975) 140.
[55] M. Machida, Y. Murata, K. Kishikawa, D. Zhang, K. Ikeue, Chem. Mater. 20 (2008) 4489–4494.